# Science Advances

## AAAS

## Supplementary Materials for

### Chemical boundary engineering: A new route toward lean, ultrastrong yet ductile steels

Ran Ding, Yingjie Yao, Binhan Sun, Geng Liu, Jianguo He, Tong Li, Xinhao Wan, Zongbiao Dai, Dirk Ponge, Dierk Raabe, Chi Zhang, Andy Godfrey, Goro Miyamoto, Tadashi Furuhara, Zhigang Yang, Sybrand van der Zwaag, Hao Chen*

*Corresponding author. Email: hao.chen@mail.tsinghua.edu.cn

**This PDF file includes:**

# Supplementary Materials



**Fig. S1. Dilatometry study and inverse pole figure maps of austenite.** (**A**) Dilatometry curves of the as-cold rolled material and the ART-ed material during fast heating and cooling. The heating and cooling rates are both 100 °C/s. Inverse pole figure maps of austenite of (**B**) the ART processed steel and (**C**) the CBE processed steel. The orientation of austenite grains in the ART processed steel is random, while after ultrafast heating and quenching neighboring austenite share the same orientation. The likely prior austenite boundaries are marked by dashed lines. During fast heating to the fully austenitic state, all PBs and most GBs disappear, while the CBs separate the coarsened austenite into densely spaced domains with different Mn concentrations.
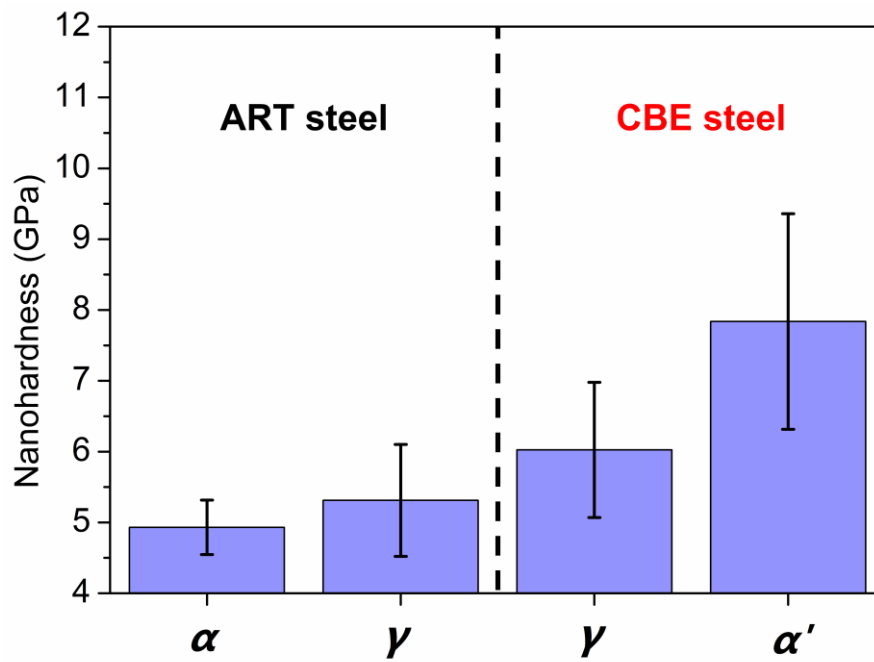
**Fig. S2. Nanohardness of each phase in ART and CBE steels.**
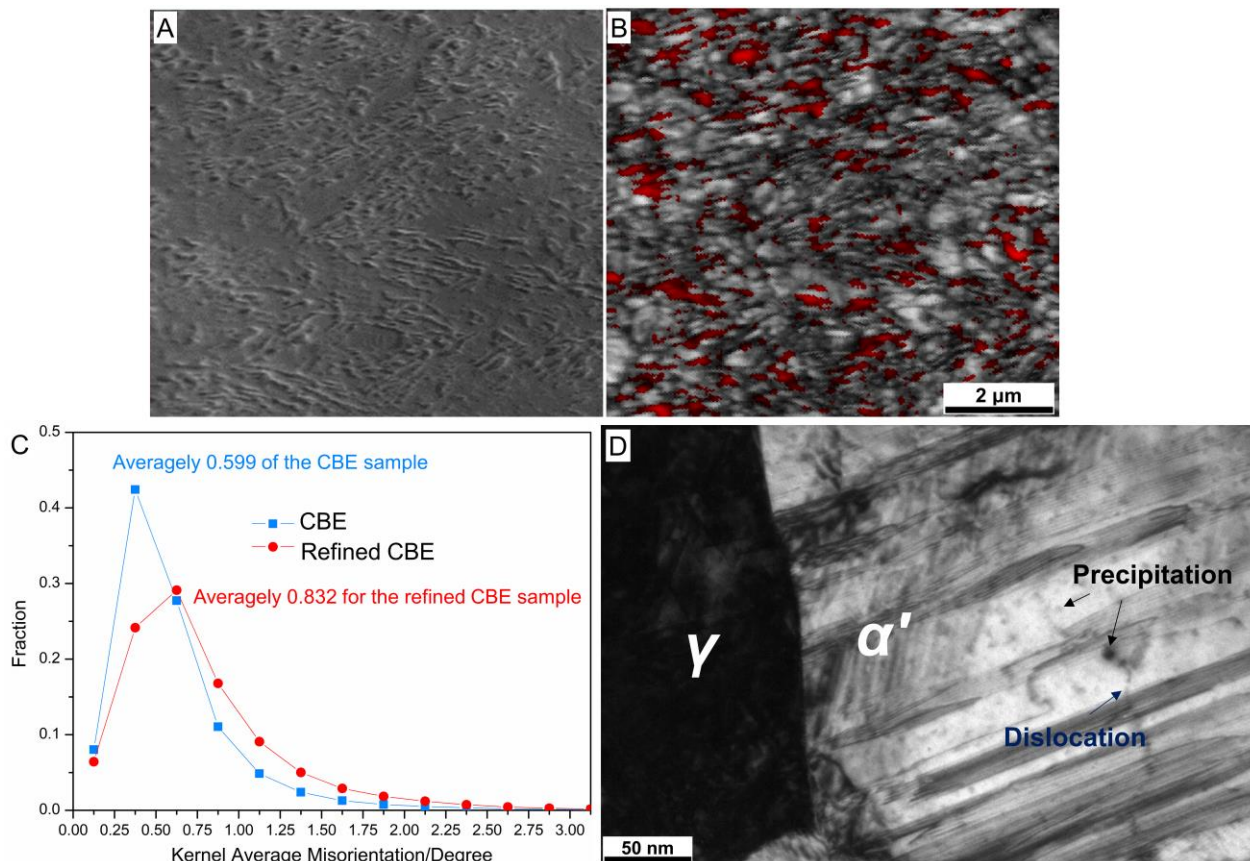


**Fig. S3. Microstructures of refined CBE steel and microalloyed CBE steel.** (**A**) SEM and (**B**) EBSD image quality map with superposed phase color map of the retained austenite (red region) of the refined CBE sample. The mean grain diameter of the retained austenite is near 160 nm. (**C**) The number fraction distributions of the KAM value in CBE and refined CBE steels (The acquired data includes both martensite and retained austenite). The dislocation density is increased in the refined CBE steel. (**D**) TEM image of microalloyed CBE steel showing dense precipitation.
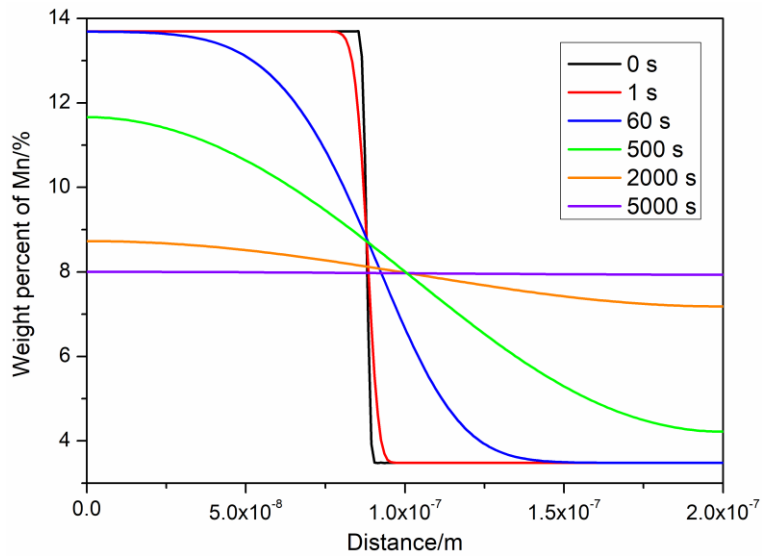
**Fig. S4. DICTRA simulation of the spatial stability of a CB inside austenite at 800°C.** The sizes of the simulation cell, of the Mn-enriched/Mn-depleted domains and the initial Mn concentration profile are taken from the experimental results presented in **Fig.2**. A Mn discontinuity with a width of ~4 nm is set at the beginning of the simulation. The apparent initial discontinuity does not fully disappear until ~5000 s.
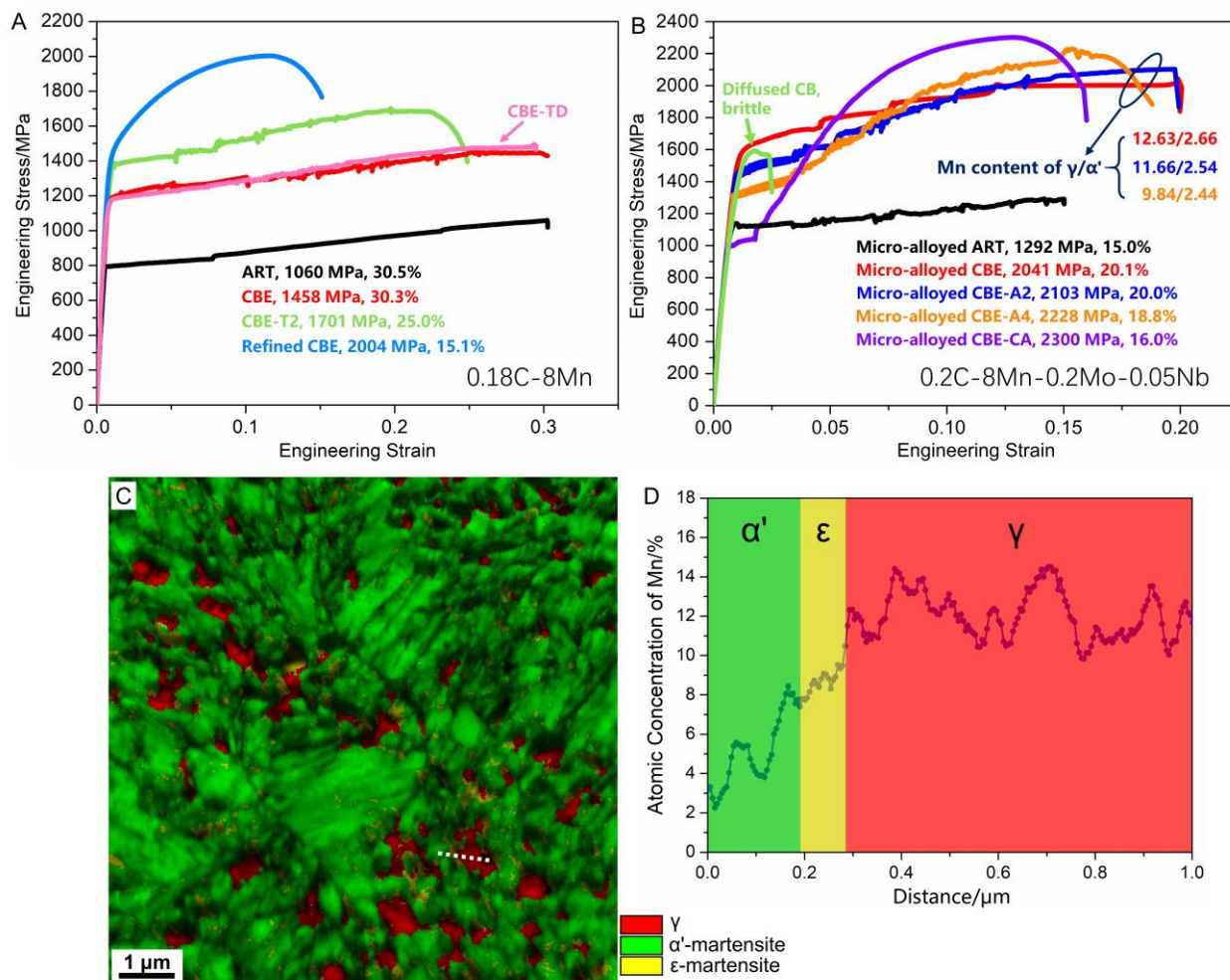
**Fig. S5. Extended mechanical properties.** (**A**) 0.18C-8Mn steel and (**B**) 0.2C-8Mn-0.2Mo-0.05Nb steel showing the wide available property range that can be achieved by CBE. The CBE-T2 sample shares the same ART and fast heating and quenching process as the CBE sample but with different tempering temperature of 300 °C. The micro-alloyed CBE-A2 and micro-alloyed CBE-A4 samples share the same fast heating and quenching process and tempering process as the micro-alloyed CBE sample but with different pre-ART temperatures of 620 and 640 °C, respectively, to tweak the Mn concentration difference across CB. The predicted Mn contents of α' and γ in micro-alloyed CBE, micro-alloyed CBE-A2 and micro-alloyed CBE-A4 samples are given as calculated using the TCFE7 thermodynamic database in the Thermo-calc software. The micro-alloyed CBE-CA sample was processed using a modified ART process developed by our group (*37*) to generate austenite with multiple composition gradients to further increase the chemical heterogeneity of the material. The steel is firstly ART-ed at 680 °C for 2 hours and ART-ed again at 600 °C for 2 hours. The subsequent fast heating, quenching and tempering process is the same as for the CBE steel. The CBE-TD sample shares the same heat treatment as the CBE sample but the tensile direction is perpendicular to the rolling direction, and shows negligible mechanical anisotropy for the CBE-processed steels. The diffused CB sample shares the same ART process as the micro-alloyed CBE sample, followed by fast heating to 800 °C and holding for 1 min, with final quenching and tempering at 400 °C for 1 min. (**C**) EBSD phase map combined with image quality map of the microstructure of the diffused CBE sample. ε-martensite formed between α'-martensite and austenite. (**D**) Mn concentration profile obtained by nano-Auger line scan along the white line in **C** indicating that the diffused CB thickness favors brittle ε-martensite formation inside thick transition regions. From a thermodynamic view, the termination of martensitic transformation at CBs is due to the rapidly decreasing driving force for

both nucleation and growth across the Mn discontinuity. However, as the effect of chemical gradients on the progress of the martensitic growth front has rarely been studied in the literature, the atomic or nanoscale mechanism behind the interaction between CBs and the displacive martensitic plate are still required to be further investigated.

**Table S1. Chemical composition of the studied alloys in weight %.**

| Steel | C | Mn | Mo | Nb | Si | Al | P | S | Fe |
|---|---|---|---|---|---|---|---|---|---|
| 0.18C-8Mn | 0.18 | 7.98 | - | - | 0.013 | <0.02 | 0.003 | 0.005 | Bal. |
| 0.2C-8Mn-0.2Mo-0.05Nb | 0.20 | 8.06 | 0.20 | 0.050 | 0.019 | <0.02 | 0.005 | 0.002 | Bal. |